plaque (n=11), calcified plaque (n=31), and media (n=27) areas.

75% of these data are used as training data for the SOM, and the rest of these data are used as test data. The SOM learned from the AR spectrum parameters of training data. And the SOM was validated by classification of training data and test data.

The SOM learned from training data and each neuron of the SOM labeled from training data are showed in Figure 1. As shown figure 1, each kinds of training data are organizing one area. This result suggests the setting of training data was reasonable.

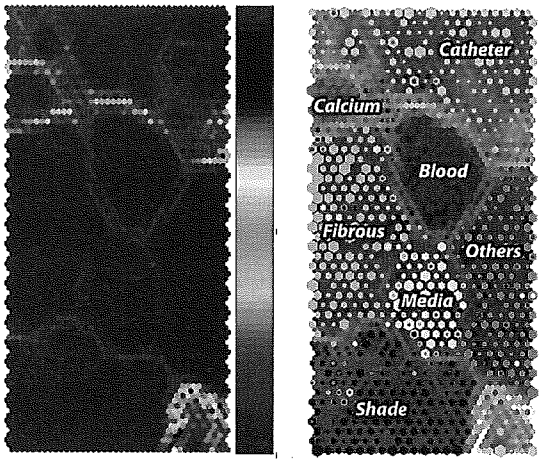

Figure 1. leaned SOM and labeld SOM

The sensitivity and specificity of classified training data by the SOM were showed in table I. There are high sensitivity and Specificity except media.

TABLE I. SENSITIVITY AND SPECIFICITY OF CLASSIFIED ROIS BY THE SOM(TRAINING DATA)

Kinds	Sensitivity	Specificity
Blood	100.0%	99.9%
Calcium	98.2%	100.0%
Catheter	99.8%	99.65%
Fibrous	94.2%	98.6%
Media	85.9%	98.4%
Others	97.0%	98.9%
Shade	89.8%	98.5%

The results of test data are showed in table II. Test data were not used as training data of SOM. So, classification of test data is the validation of the SOM classifier.

TABLE II. SENSITIVITY AND SPECIFICITY OF CLASSIFIED ROIS BY THE SOM(TEST DATA)

Kinds	Sensitivity	Specificity
Blood	100.0%	99.8%
Calcium	88.5%	99.8%
Catheter	99.2%	99.8%
Fibrous	88.3%	98.8%
Media	74.4%	96.7%
Others	92.8%	98.6%
Shade	88.3%	96.8%

Color-code map that classified whole echogram by the SOM is showed in figure 2 and figure 3. On the left hand side of figures 2 and 3 are the original echograms, and on the right hand side are color-code maps with the classification of each area of these echogram by the SOM.

In the figure 2, numbers of color bar are as follow: 1 is others, 2 is blood, 3 is fibrous plaque, 4 is shade of guide wire, 5 is blood, 6 is calcified plaque, 7 is media, and 8 is catheter. In the figure 3, numbers of color bar are as follow: 1 is catheter, 2 is others, 3 is shade of guide wire, 4 is blood, 5 is fibrous plaque, 6 is media, and 7 is calcified plaque.

The SOM classified well the inner lumen of figure 2, but not classified the outside of lumen. Because the SOM was not trained with data of outside of lumen.

The SOM did not classify well the image in the figure 3. In this image, the SOM classified area of inner lumen, media as fibrous plaque.

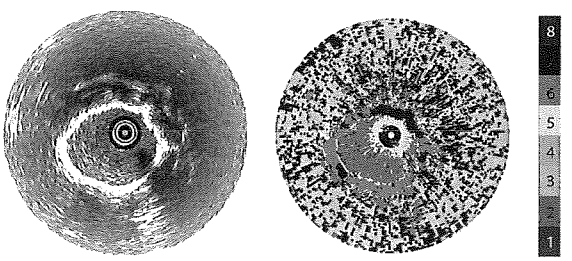

Figure 2. echogram and color-code map

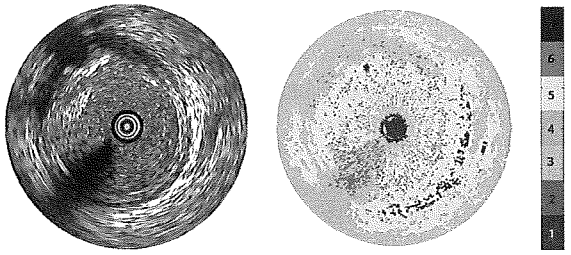

Figure 3. echogram and color-code map

IV. CONCLUSIONS

In this study, we classified IVUS RF data of coronary tissues using a SOM classifier based on multiple spectrum parameters.

The accuracies for classification of IVUS RF data were 95.9% for fibrous plaque region, 99.5% for blood region, 96.2 % for calcified plaque region, and 16.3 % for media regions. These results showed that the SOM classifier has potential for characterization of coronary tissues.

In future studies, with further data collection, we plan to develop statistically stable and robust classification rules for prediction of atherosclerotic plaque formation.

ACKNOWLEDGMENT

This study was supported by Grants-in-aid from Japan Society for Promotion of Science (15300178) and Grants-in-aid from Ministry of Health, Labour and Welfare (H17-nano-001).

REFERENCES

] Klingensmith J, Vince D, Kuban B, et al. Assessment of coronary compensatory enlargement by three-dimensional intravascular ultrasound. Int J Card Imaging. 2000. vol.16. pp.87-98.

] Nissen SE, Gurley JC, Grines CL, et al. Intravascular ultrasound assessment of lumen size and wall morphology in normal subjects and patients with coronary artery disease. Circulation. 1991. vol.84 pp.1087-1099.

] Schoenhagen P, Ziada KM, Kapadia SR, et al. Extent and direction of arterial remodeling in stable versus unstable coronary syndromes. Circulation. 2000. vol.101. pp.598-603.

[4] Tuzcu EM, Hobbs RE, Rincon G, et al. Coronary heart disease/ myocardial infarction: occult and frequent transmission of atherosclerotic coronary disease with cardiac transplantation: insights from intravascularultrasound. Circulation. 1995. vol.91. pp.1706-1713.

[5] Von Birgelen C, de Vrey EA, Mintz GS, et al. ECG-gated threedimensional intravascular ultrasound: feasibility and reproducibility of the automated analysis of coronary lumen and atherosclerotic plaque dimensions in humans. Circulation. 1997. vol.96. pp.2944-2952.

[6] Nissen SE, Yock P. Intravascular ultrasound: novel pathophysiological insights and current clinical applications. Circulation. 2001. vol.103. pp. 604-616.

[7] Baldeweck T, Laugier P, Herment A, et al. Application of utoregressive spectral analysis for ultrasound attenuation estimation: interest in highly attenuating medium. IEEE Trans Ultrason Ferroelectrics Frequency Control. 1995;42:99–110.

[8] Kay SM. Modern spectral estimation. Theory and application. Englewood Cliffs, NJ: Prentice Hall, 1988.

[9] T.Kohonen, Self-Organizing Map, 3rd Edition, Springer, 2004.

[10] T. Kohonen, "New developments of learning vector quantization and the self-organizing map", SYNAPSE'92, Symposium on Neural Networks; Alliances and Perspectives in Senri 1992, Osaka, Japan, June 24–26, 1992.

[11] Metz CE. Basic principles of ROC analysis. Semin Nucl Med. 1978;8: 283–298.

Luminal Contour Detection in Intravascular Ultrasound Images

E. Santos Filho[1], M. Yoshizawa[2], A. Tanaka[3], Y. Saijo[4], T. Iwamoto[1]

1 Graduate School of Engineering, Tohoku Univ., Aoba 6-6-05, Aoba-ku, Sendai 980-8579, Japan

2 Information Synergy Center, Tohoku Univ., Aoba 6-6-05, Aoba-ku, Sendai 980-8579, Japan

3 College of Symbiotic Systems Science, Fukushima Univ., Kanayagawa 1, Fukushima 960-1296, Japan

4 Inst. of Development, Aging and Cancer, Tohoku Univ., Seiryo-machi, Sendai 980-8575, Japan

santos@yoshizawa.ecei.tohoku.ac.jp

Abstract: A system for luminal contour segmentation in intravascular ultrasound images is proposed. Moment based texture features together with the radial distance feature are used for clustering of the input image pixels. After the clustering, morphological smoothing and boundary detection process are applied and the final image is obtained. The proposed method was applied to 15 images of different patients and a correlation coefficient equal to 0.86 was obtained between the areas of lumen automatically and manually defined.

Keywords: image segmentation, texture, ultrasound.

1. Introduction

Cardiovascular pathologies are one of the main causes of mortality in the Western world. Atherosclerosis, disease of intima layer of the artery, represents the essential characteristic of arterial pathologies[1]. Atherosclerosis consists of lipids, complex carbohydrates, blood cells, fibrous tissues and calcified deposits, forming a plaque that occludes progressively the lumen of the artery. A number of imaging modalities exist to help diagnosis coronary artery diseases. Among them, X-ray coronary angiography and intravascular ultrasound (IVUS) represent the most commonly used diagnostic tools.

Segmentation of deformable structures is a common processing problem in medical imaging. For example, coronary artery atherosclerosis severity is mainly deduced from the degree of vessel stenosis induced by the atherosclerotic plaque formation. It is generally estimated, from IVUS images, by segmenting and measuring the lumen area, and by referencing it to the total cross-sectional area of the vessel. With the majority of IVUS systems, this work is generally performed manually. However, due to tedious nature of manual tracing, many research groups have worked on developing semi-automatic and automatic segmentation and analysis methods in IVUS images as well as angiography.

Brusseau *et al.*[2] developed a fully automatic method for luminal contour that evolves until it optimally separates regions with different statistical properties. Their system used a phase array transducer and achieved a high level of accuracy. However, no mention was made of the widely used rotating systems.

Bovenkamp *et al.*[3] developed an automatic multi-agent-based system for luminal contour segmentation. Each agent cooperates with other agents to come to a consistent overall image segmentation. However, the complexity of this system may lead to time delays when there is a conflict among the agents.

Tuceryan[4] proposed a method for obtaining texture features directly from gray-level images by computing the moments of the image in local regions. The results of his segmentation algorithm show that the image moments computed over local regions provide a powerful set of features that reflect certain textural properties in images.

In this papers, like those by Brusseau[2] and Bovenkamp[3], we proposed a system for automatic luminal contour segmentation. Unlike the Brusseau system,[2] our system is applied to images obtained from a rotating IVUS system due to the fact that these systems are widely used in clinical settings. Instead of a multi-agent system, as proposed by Bovenkamp[3], we used the simpler and more powerful set of features proposed by Tuceryan[4] to achieve our goal of luminal contour segmentation.

Our strategy to achieve this goal is to extract local moment based texture features and a pixel position feature from IVUS images to perform a clustering on the basis of these features. Once we obtain the clustered image, a smoothing filter is applied to reduce the irregularities of the boundary and then the final segmentation is carried out. This process is illustrated in Fig.1.

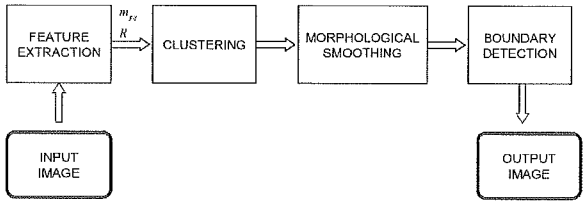

Fig.1 – Block diagram of the proposed system for luminal contour segmentation

PR0001/05/0000-1076 ¥400

2. Materials and Methods

Our texture segmentation algorithm is based on Tuceryan's work[4] and consists of the following steps: (a) compute the image moments within a small window around each pixel as well as the radial distance of each pixel, (b) compute the texture features from these moments by applying a nonlinear transformation followed by an averaging operation, (c) perform a fuzzy clustering of the pixels of the input image on the basis of these features, and (d) classify every pixel in the image according to the minimum distance from the centers of the clusters found in step (c).

In this system the input image is the original image obtained from the IVUS system. We used a commercial available IVUS system (Clear View Ultra, Boston Scientific, USA). The central frequency of the rotating IVUS probe (Atlantis SR Pro, Boston Scientific, USA) was 40 MHz.

2.1 Moments

Our algorithm uses the moments of an image to compute texture features. The $(p+q)$-th order moment m_{pq} of a function of two variables $f(x,y)$ with respect to the origin (0,0) is defined as[2]:

$$m_{pq} = \int_{-\infty}^{\infty}\int_{-\infty}^{\infty} f(x,y)x^p y^q dxdy \qquad (1)$$

where p,q = 0,1,2, ... Normally the moments are computed over some bounded region. If the function is equal to unity within the region and zero outside the region, the lower order moments (small values of p and q) have well defined interpretations. For example, m_{00} is the area of the region, m_{10} / m_{00} and m_{01} / m_{00} give the x and y coordinates of the centroid for the region, respectively. The m_{20}, m_{11} and m_{02} can be used to derive the amount of elongation o the region, and the orientation of its major axis. The higher order moments give even more detailed shape characteristics of the polygons such as symmetry, etc.

In this paper, as in Tuceryan's work[4], we regard the intensity image as a function of two variables, $f(x,y)$. We compute a fixed number of lower order moments for each pixel in the image (we use $p+q \le 2$). The moments are computed within a small local window around each pixel.

Given a window size W, the coordinates are normalized to the range of [-0.5 , 0.5] and the pixel is located at the center. The moments are computed with respect to this normalized coordinate system. This permits us to compare the set of moments computed for each pixel. We always choose the window width W to be odd so that the pixel (i , j) is centered on a grid point.

Let (i , j) be the pixel coordinates for which the moments are computed. For a pixel with coordinates (k , l) that fall within the window, the normalized coordinates (x_k, y_l) are given by:

$$x_k = \frac{k-i}{W} \qquad y_l = \frac{l-j}{W} \qquad (2)$$

Then the moment $m_{pq}(i,j)$ within a window centered at pixel (i,j) is computed by a discrete sum approximation of Equation (1) that uses the normalized coordinates (x_k, y_l):

$$m_{pq}(i,j) = \sum_{k=-W/2}^{W/2}\sum_{l=-W/2}^{W/2} f(i+k, j+l)x_k^p y_l^q \qquad (3)$$

This discrete computation of the set of moments for a given pixel over a finite rectangular window corresponds to a neighbor operation, and, therefore, it can be interpreted as a convolution of the image with a mask[4].

When we examine the masks, we see that they can be interpreted as local features detectors. For example, the mask for m_{00} corresponds to a box-averaging window, and thus it can be interpreted as computing the total energy within that box. The masks for m_{10} and m_{01} take the form of edge detectors. They would respond to sudden intensity changes in the x and y directions, respectively. The second order moments are not easy to interpret; the only exception being m_{11}, which looks like a cross detector[4].

The set of values for each moment over the entire image can be regarded as a feature image. Let M_k be the k-th such image. If we use n moments, then there will be n such moments images. In our experiments, we used m_{00}, m_{01}, m_{10}, m_{11}, m_{02}, and m_{20}, which result in the images M_1, M_2, M_3, M_4, M_5, and M_6, respectively.

2.2 Radial distance

In this work, we define the radial distance R as the distance from the central pixel of the image to the position of the pixel P under consideration. This distance R is the seventh feature (together with m_{00}, m_{01}, m_{10}, m_{11}, m_{02}, and m_{20}) used in the following clustering of the input image pixels. Based on these features, the pixels were clustered in the clustering block using the Fuzzy C Means algorithm[5].

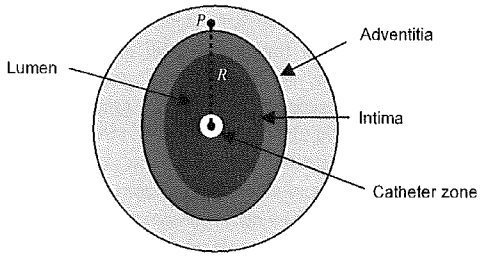

Fig.2 – Illustration of a cross-section of a blood vessel

The number of clusters chosen was four: one cluster for the external region, one for the region between the adventitia and intima, one for the lumen and another one for the catheter zone. After the clustering the image could have its boundaries easily detected by any boundary detection method. However, in order to reduce the irregularities of the borders as well as some small regions around the borders, a

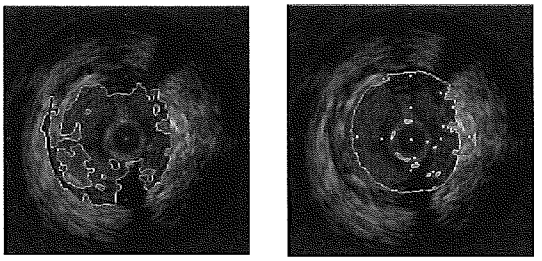

(A) (B)

Fig.3 – Effect of the radial distance feature *R* as one of the components of the feature vector. (A) and (B) are the same images obtained from patient A. (A) Clustered image without using the radial distance feature *R*. (B) Clustered image using the radial distance feature *R*.

morphological filtering was done prior to the boundary detection.

2.3 Morphological contour smoothing

Mathematical morphology is a technique of image processing whose value for each pixel in the output image is based on a comparison of the corresponding pixel in the input image with its neighbors. By choosing the size and shape of the neighborhood, we can define a morphological operation that is sensitive to specific shapes in the input image. The neighborhood size and shape are determined by the size and shape of a second, usually much smaller, image called *structuring element*, which together with the input image is regarded as a set. Thus, basic operations of the set theory like union, subtraction and compliment can be carried out with both images. These basic operations can be used to compose other operations like *opening* and *closing*, for example. Opening generally smoothes the contour of an object, breaks narrow isthmuses, and eliminates thin protrusions. Closing also tends to smooth sections of contour, but, as opposed to opening, it generally fuses narrow breaks and long thin gulfs, eliminates small holes and fills gaps in the contour[6].

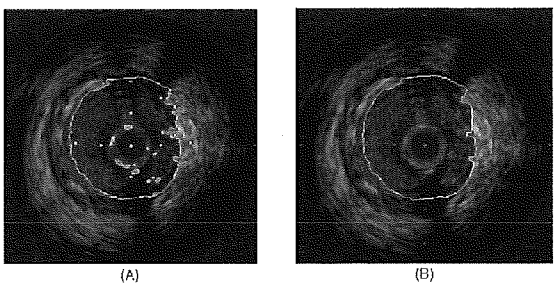

(A) (B)

Fig.4 – (A) Result of the clustering; (B) Result of the morphological contour smoothing

In order to reduce the irregularities of the borders as well as some small regions around the borders, morphological filtering is done prior to boundary detection. This filtering is performed through the application of opening and closing morphological operations with a disk structuring element of size 3. An example of the result of the luminal contour obtained from the clustering process without any contour smoothing can be seen in Fig. 4(A). An example of the luminal contour obtained when the morphological filter is applied after the clustering is shown in Fig.4(B).

3. Analysis of results

Using the system presented above, tests were done with 15 IVUS images of different patients. We can observe in Fig.6 that the boundaries automatically drawn by the proposed system closely resemble the ones drawn manually by an expert medical doctor. In Fig.5 is shown the correlation between the areas of the automatically defined lumen and manually defined lumen. The correlation coefficient was equal to 0.86.

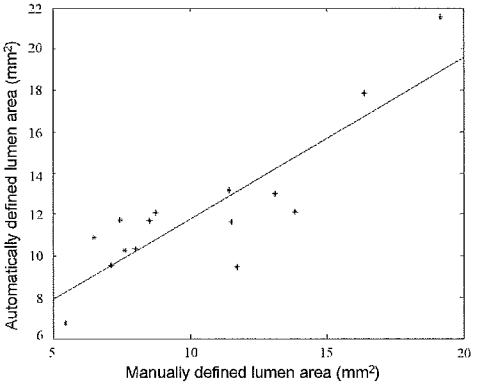

Fig.5 – Correspondence between the lumen area manually defined and the area automatically defined.

The transition between the lumen and the vessel wall as well as the transition between the vessel layers is quite smooth. This makes the boundaries detection based on local features a hard task. However, due to the ability of the local moments in characterization of textured regions, together with the radial distance, it was possible to identify the pixels that belong to the lumen region and those that do not belong. With this method only the lumen boundary detection achieved a reasonable level of accuracy. The outer vessel border was not accurately detected so far, mainly, due to the much more smooth transition from the vessel wall to surrounding tissues. To overcome this difficulty, it seems that more global features should be added to the system as has been studied by Brusseau[2] and Bovenkamp[3].

The effectiveness of the proposed radial distance feature *R* can be observed in Fig.3. In Fig.3(A) we can see an example of segmentation without using the feature *R*. We can see that in this case the resulting segmentation is more irregular and contains some sub-regions segmented inside the lumen region. This over-segmentation occurs mainly because of some texture and gray level changes inside the lumen region. When the radial distance feature is added to the clustering process, the differences among these segmented sub-regions are overcome because they acquire a feature that is similar in most of them, and then this strongly influences the clustering results.

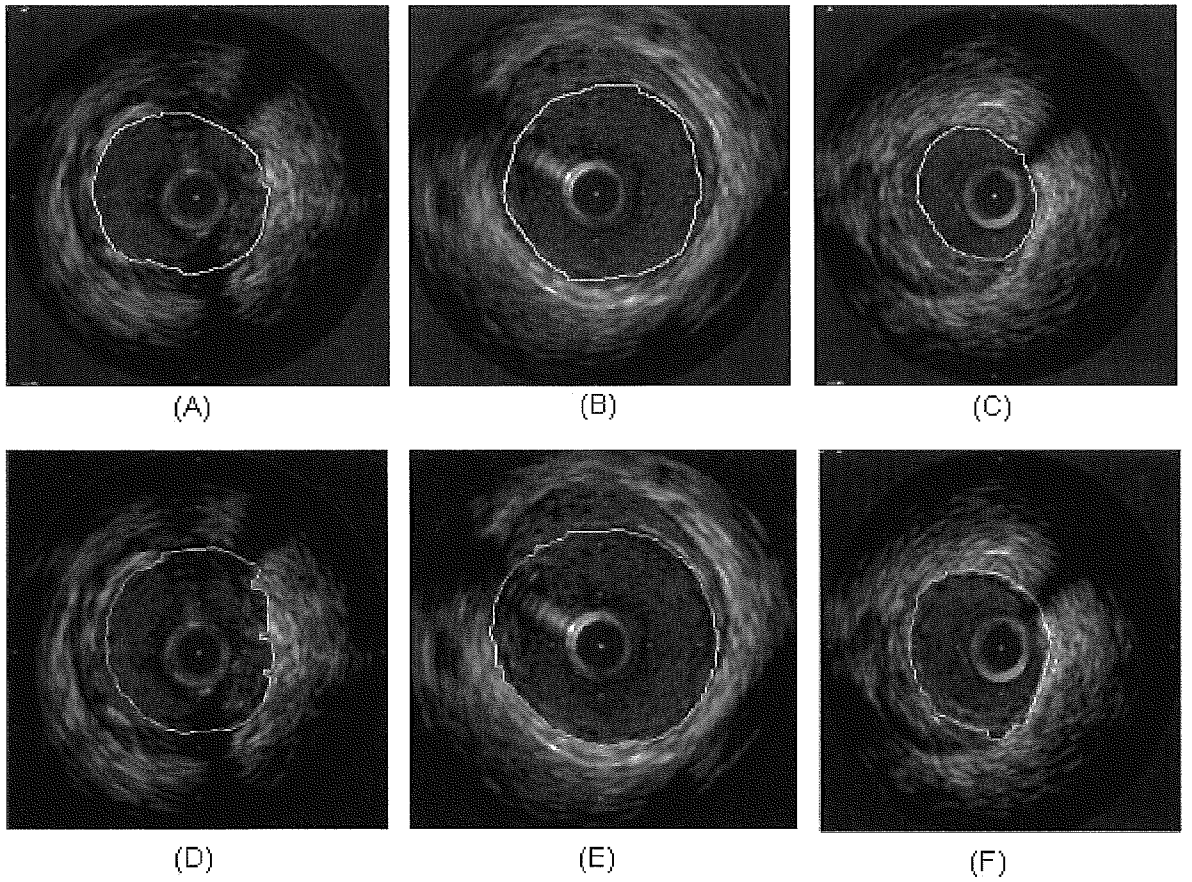

Fig. 6 - Example of luminal contour detection. (A),(B) and (C) are images manually segmented. (D),(E) and (F) are the corresponding images automatically segmented.

Thus, we can obtain a more regular and compact segmentation of the lumen region, as shown in Fig.3(B).

4. Conclusion

Based on our tests, we can conclude that the moment-based texture features together with the radial distance are feasible components for a feature vector in IVUS image segmentation when the aim is to find the luminal contour.

The process was improved when the morphological smoothing filtering was carried out after the clustering and before the boundary detection process. Tests performed with 15 images from different patients resulted in a correlation coefficient of 0.86 between the lumen areas automatically detected and lumen areas manually detected.

Only the segmentation of the luminal contour has been considered. As future work, we plan to extend this method to detection of the vessel contour, which is necessary for assessment of the degree of vessel stenosis. In pratical terms, once having determined the position of the blood-tissue interface, the luminal area will be excluded and the second contour will be searched in the remaining region.

References

[1] X. Zhang, R. Charles and M. Sonka, Tissue characterization in intravascular ultrasound images, IEEE Transaction on Medical Imaging, Vol. 17, No. 6, pp. 889-899, 1998.

[2] E. Brusseau, C.L. Korte, C.L., F. Mastik, J. Schaar and A.F.W. van der Steen, Fully automatic luminal contour segmentation in intracoronary ultrasound imaging - a statistical approach, IEEE Transactions on Medical Imaging, Vol. 23, No. 5, pp.554-566, May 2004

[3] E.G.P. Bovenkamp, J. Dijkstra, J.G. Bosch, and J.H.C. Reiber, Multi-agent segmentation of IVUS images, Pattern Recognition, Elsevier, Vol. 37, pp. 647-663, No. 4, April 2004.

[4] M. Tuceryan, Moment based texture segmentation, Proceedings of 11th IAPR International Conference on Image, Speech ,Signal Analysis and Pattern Recognition, pp.45-48, 1992

[5] J.C. Bezdek, Pattern recognition with fuzzy objective function algorithms, Plenum Press, New York, 1981

[6] R.C. Gonzalez and R. E. Woods, Digital image processing, Prentice Hall, New Jersey, 2002.

Proceedings of the 2005 IEEE
Engineering in Medicine and Biology 27th Annual Conference
Shanghai, China, September 1-4, 2005

Detection of Luminal Contour Using Fuzzy Clustering and Mathematical Morphology in Intravascular Ultrasound Images

Esmeraldo dos Santos Filho, Makoto Yoshizawa, Akira Tanaka, Yoshifumi Saijo and Takahiro Iwamoto

Abstract— **An innovative application of fuzzy clustering and mathematical morphology for the problem of luminal contour detection in intravascular ultrasound images is presented. Median and standard deviation are used as features for segmentation process. Comparison was made with gold standard segmented images obtained from the average of images segmented by experienced medical doctors. Tests were carried out with 20 *in vivo* coronary images obtained from different patients. High correlation coefficients were found between lumen regions manually and automatically defined when area, mean gray level, and standard deviation of the lumen regions were compared.**

I. INTRODUCTION

Cardiovascular pathologies are one of the main causes of mortality in the Western world. Atherosclerosis is a disease in which the arteries are hardened and narrowed due to the gradual build-up of plaque on their inner wall.

The intravascular ultrasound (IVUS) is a catheter-based technique that generates cross-sectional images of the lumen, plaque and vessel wall. Coronary artery atherosclerosis severity is mainly deduced from the degree of vessel stenosis induced by the atherosclerotic plaque formation. It is generally estimated, from IVUS images, by segmenting and measuring the lumen area, and by referencing it to the total cross-sectional area of the vessel. With the majority of IVUS systems, this work is generally performed manually. However, due to the tedious nature of manual tracing, many research groups have worked on developing automatic segmentation methods for IVUS images.

Brusseau *et al* [1] developed a fully automatic method for luminal contour segmentation in IVUS images based on an active contour that evolves until it optimally separate regions with different statistical properties. Their system used a phase array transducer and achieved high accuracy level. However, no mention was done about the case of the largely used rotating systems.

Bovenkamp *et al* [2] developed an automatic multi-agent based system for luminal contour segmentation. Each agent cooperates with other agents to come to a consistent overall image segmentation. However, the complexity of this system may lead to time delay in case of conflict among the agents.

This work was supported by Health and Labor Sciences Research Grants H15-Fiji-001 of Ministry of Health Labor and Welfare of Japan and the Grant of Tohoku University 21 COE Program: 'Future Medical Engineering based on Bio-nanotechnology'.

Esmerado dos Santos Filho is with Graduate School of Engineering, Tohoku University, Aoba 6-6-05, Aoba-ku, Sendai 980-8579, Japan (esmeraldo@ieee.org)

Makoto Yoshizawa is with Information Synergy Center, Tohoku University, Japan (yoshizawa@ieee.org)

Akira Tanaka is with College of Symbiotic Systems Science, Fukushima University, Japan (a-tanaka@ieee.org)

Yoshifumi Saijo is with Institute of Developement, Aging and Cancer, Tohoku University, Japan (saijo@idac.tohoku.ac.jp)

Takahiro Iwamoto is with Graduate School of Engineering, Tohoku University, Japan (iwamoto@ecei.tohoku.ac.jp)

0-7803-8740-6/05/$20.00 ©2005 IEEE.

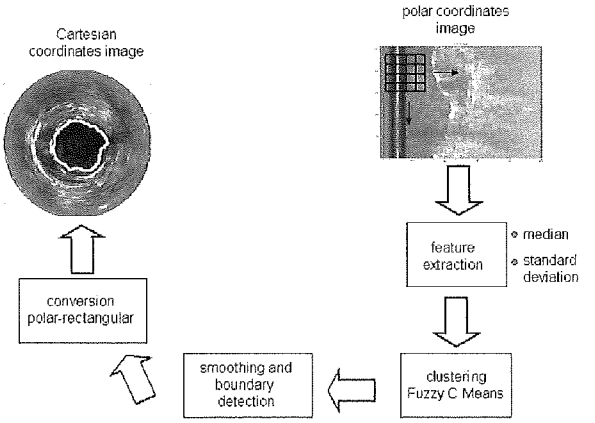

Fig. 1. Block diagram of the proposed algorithm for luminal contour segmentation

In this paper, like those by Brusseau [1] and Bovenkamp [2], we proposed a system for automatic luminal contour segmentation. Unlike the Brusseau's system [1] our system is applied on images obtained from a rotating IVUS system due to the fact that these systems are largely used in clinical settings. Instead of a multi-agent system, as proposed by Bovenkamp [2], we used a fuzzy clustering based in on simple statistics, mean and standard deviation, obtained from a sliding window that scans the entire input image.

II. MATERIALS AND METHODS

In this work, we used a commercial available IVUS system (Clear View Ultra, Boston Scientific, USA). The central frequency of the rotating IVUS probe (Atlantis SR Pro, Boston Scientific, USA) was 40 MHz.

After the acquisition the RF signal was used to generate polar coordinate system images to facilitate the search for the lumen boundary. A block diagram of the proposed system is shown in Fig.1

A. Feature extraction and fuzzy clustering

Using a 7×7 sliding window, the input polar coordinate system image was scanned from the left to the right and from top to bottom. For each position of this window the median and standard deviation of the gray level of the pixels included in the window were calculated and became the features used

to represent the pixel in the center of the window. This process was repeated for every pixel of the input image.

The Fuzzy C-means algorithm [3] was used for clustering of the pixels of the input image on basis of their median and standard deviation features. The number of clusters was defined equal to two: one for lumen region and one for the vessel and external region. The catheter zone was ignored during the clustering process.

One example of the clustering result can be seen in Fig.2. In Fig2(A) we have an example of polar coordinate system input image and in Fig.2(B) is shown the corresponding clustered image.

B. Smoothing and boundary detection

After the clustering a morphological filter was applied to eliminate some irregularities of the image and small segmented regions as well. Thus, the clustered image was first submitted to an operation of region filling followed by closing with disk structuring element of size 5. This filtering helped to obtain a more regular boundary as shown in Fig.2(C).

After the morphological filtering the boundary between lumen and vessel was detected by scanning the filtered image from the left to the right until the transition from black to white be found and then, immediately, jumping to the next line. With this procedure was possible detect the lumen boundary as shown in Fig.2(D). After that the lumen boundary was converted to Cartesian system , as shown in Fig.2(E), and superposed on the original image as shown in Fig.2(F).

C. Evaluation method

In order to evaluate the accuracy of the performed segmentation, the results should be compared with the real lumen shape. Because the actual shape is not known, a gold standard reference image is obtained from manual segmentations.

The manual segmentation results show variability between different observers and sometimes also between the two

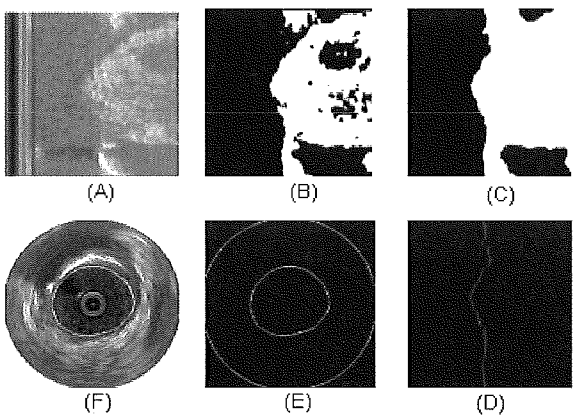

Fig. 2. Example of automatically segmented image. (A) Polar coordinate system input image. (B) Clustered image. (C) morphologically filtered image. (D) Detected lumen boundary. (E) Lumen boundary converted to Cartesian system. (F) Final output image.

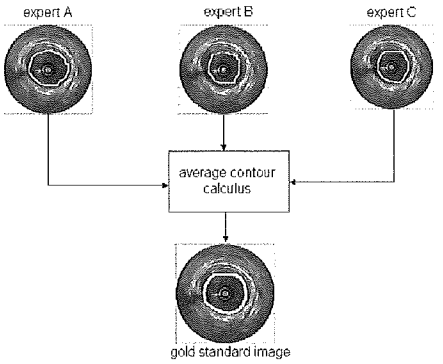

Fig. 3. Block diagram of gold standard generation procedure

traces of one observer, so a single manual segmentation cannot act as a standard. We therefore derive a gold standard reference image by calculating the average shape of the manual segmentations using shape-based interpolation [5]. This technique uses the shapes of the binary object in each manual segmentation to calculate so-called distance scenes. In a distance scene, each pixel is given a value the represents the nearest pixel of the object, i.e., the lumen contour. Pixels inside the lumen are given negative distance values.

The average shape is then calculated by adding the distance scenes of all manual segmentations; the transition from positive to negative values yields the average contour as has been done in Bouma's work [6]. In this work we used images segmented by three experienced medical doctors to generate the gold standard images as illustrated in Fig.3.

In order to obtain a reliable comparison, the automatically segmented images as well as their corresponding gold standard were divided in four quadrants similarly as has been proposed by Allonso's work [7]. An example is shown in Fig.4. For each quadrant the variance, mean gray level, and area were calculated. The correlation between the features extracted from the gold standard and the corresponding features extracted from automatically segmented images are shown in Fig.5,6, and 7.

III. RESULTS AND DISCUSSION

Using the system presented above, tests were done with 20 *in vivo* coronary IVUS images from different patients. Fig.5,6, and 7 show the correlation between features of the automatically defined lumen regions and manually defined lumen region. The correlation coefficient was equal to 0.94

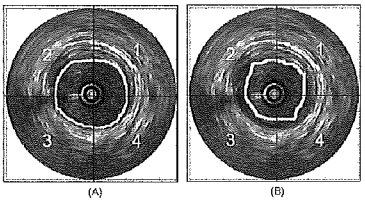

Fig. 4. Example of images divided in quadrants for comparison

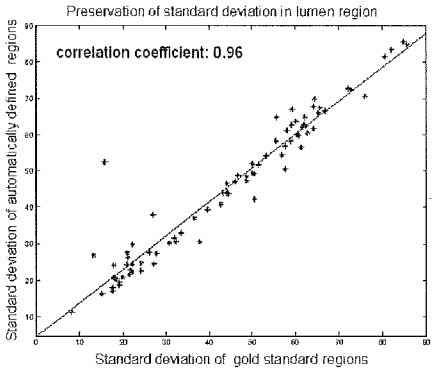

Fig. 5. Correspondence between the standard deviation of the pixels gray level calculated in the lumen region manually defined and the lumen region automatically defined

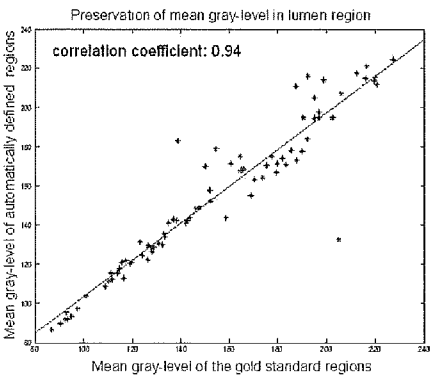

Fig. 6. Correspondence between the mean gray level calculated in the lumen region manually defined and the lumen region automatically defined

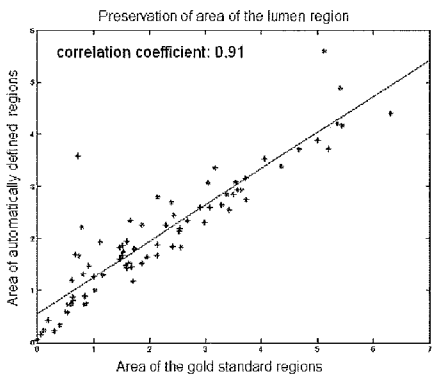

Fig. 7. Correspondence between the lumen area manually defined and the area automatically defined

for the feature mean gray-level, 0.96 for the feature standard deviation, and 0.91 for the feature area.

Some examples of the results are shown in Fig.8 together with the corresponding gold standard images comparison. We can observe that the images segmented automatically by the proposed algorithm closely resemble the gold standard ones.

Some tests were also carried out using images obtained from phantoms due to the fact that in the phantom images the lumen contour is easily detected visually and then may be used for asses the accuracy of the proposed segmentation method. An example que be seen in Fig.9.

The morphological filtering together with the method for search for boundary described in Section II-B were effective in finding the lumen border. This process could be easily performed in the polar coordinate system image but would be not so easy to perform in the Cartesian system image usually used.

The proposed algorithm cannot detect the external vessel contour due to the much more smooth transition between the external vessel wall and the surrounding tissues and the lack of contrast. It seems that more high-level knowledge should be added to the system to make it possible to detect the vessel external contour.

IV. CONCLUSIONS

A system for automatic segmentation of luminal contour was presented. The segmentation was performed through fuzzy clustering using the median and standard deviation of the pixels inside a sliding window as pixel features. After the clustering a morphological filtering was done and the lumen boundary was detected. This method presented high level level of accuracy when compared with gold standard segmented images. However, only the luminal contour was detected. As future work, we plan to extend this method to detection of the vessel contour, which is necessary for assessment of the degree of vessel stenosis. In practical terms, once having determined the position of the blood-tissue interface, the luminal area will be excluded and the second contour will be searched in the remaining region.

REFERENCES

[1] E. Brusseau, C.L. Korte, F. Mastik, J. Schaa and A.F.W. van der Steen, Fully automatic luminal contour segmentation in intracoronary ultrasound imaging - a statistical approach, *IEEE Trans. on Medical Imaging*, vol. 23, 2004, pp.554-566.

[2] E.G.P. Bovenkamp, J. Dijkstra, J.G. Bosch and J.H.C. Reiber, Multi-agent segmentation of IVUS images, *Pattern Recognition*, vol.37, 2004, pp.647-663.

[3] J.C. Bezdek,*Pattern recognition with fuzzy objective function algorithms*,Plenum Press, New York; 1981.

[4] R.C. Gonzales and R.E. Woods, *Digital image processing*,Prentice Hall, New Jersey; 2002.

[5] S.P. Raya and J.K. Udupa, Shape-based interpolation of multidimensional objects, *IEEE Trans. Medical Imaging*, vol.9, 1990, pp.32-42.

[6] C.J. Bouma, W. J. Niessen, K. J. Zuiderveld, E. J. Gussenhoven and A. Viergever, Automated lumen definition from 30 MHz intravascular ultrasound images, *Medical Image Analysis*, vol.1, 1997, pp.363-377.

[7] F. Alonso, M.E. Algorri, F. Flores-Mangas, Composite Index for the quantitative evaluation of image segmentation results, *Proceedings of the 26th Annual International Conference of the IEEE EMBS*, San Francisco, CA, USA, 2004, pp.1794-1797.

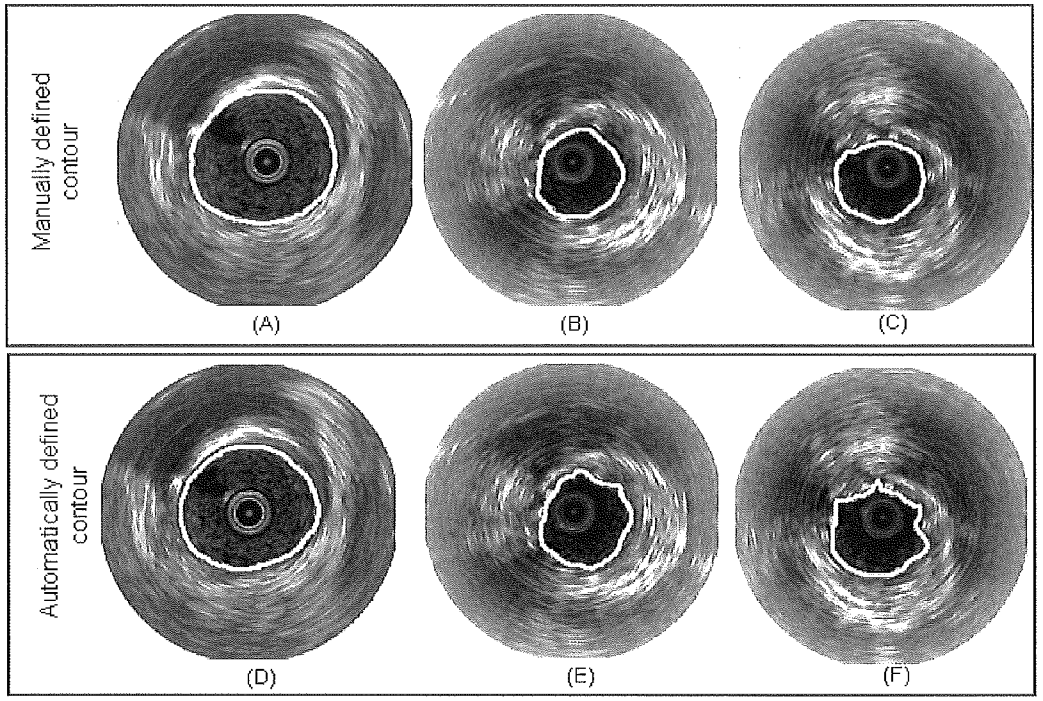

Fig. 8. Comparison between images automatically segmented and gold standard segmented images

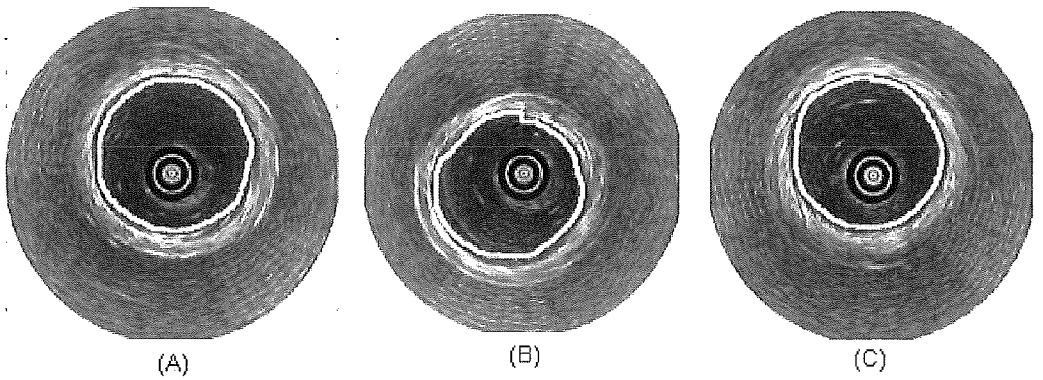

Fig. 9. Examples of automatically segmented images obtained from phantoms

8th Sendai Symposium on Ultrasonic Tissue Characterization

November 11, 2005, 10:00 – 18:00

Institute of Development, Aging and Cancer, Tohoku University

Morning Sessions

Novel Approaches in Intravascular Ultrasound

Parametric Intravascular Ultrasound Imaging
Yoshifumi Saijo (*Institute of Development, Aging and Cancer, Tohoku University*)

Automatic Luminal Contour and Calcification Detection in Intravascular Ultrasound Images
Esmeraldo dos Santos Filho (*Institute of Development, Aging and Cancer, Tohoku University*)

Precise Ultrasonic Measurement of Biological Materials

Elasticity Imaging of Artery Wall for Transcutaneous Tissue Characterization
Hideyuki Hasegawa (*Graduate School of Engineering, Tohoku University*)

Ultrasonic Measurement of Displacement Inside Object Caused by Dual Acoustic Radiation Force
Mikito Takahashi (*Graduate School of Engineering, Tohoku University*)

Afternoon Sessions

Elasticity Measurement of Myocardium

Noninvasive Measurement of Myocardial Viscoelasticity
Hiroshi Kanai (*Graduate School of Engineering, Tohoku University*)

Measurement of Myocardial Strain Rate at High Temporal Resolution
Hiroki Yoshiara (*Graduate School of Engineering, Tohoku University*)

Development of Novel Acoustic Microscopy

Speed-of Sound Microscopy for Biomedical Applications
Yoshifumi Saijo (*Institute of Development, Aging and Cancer, Tohoku University*)

Image processing for pulse driven biological microscope based on frequency spectrum
Ayumi Kimura (*Toyohashi University of Technology*)

Recent Applications of Acoustic Microscopy in Orthopedic Surgery

Increased Sound Speed of Synovial Membrane after Immobilization Assessed by Scanning Acoustic Microscopy
Yoshihiro Hagiwara (*Department of Orthopaedic Surgery, Tohoku University*)

Material Properties of the Rabbit Supraspinatus Tendon and its Insertion - A Measurement with the Scanning Acoustic Microscopy
Hirotaka Sano (*Department of Orthopedic Surgery, Tohoku University*)

Invited Lecture (17:00 –18:00)

Intravascular Ultrasound for Studying Atherosclerotic Plaque

Professor A. F. W. van der Steen (*Department of Biomedical Engineering, Thorax Centre, Erasmus Medical Center, Rotterdam)*

担当：病態計測制御分野　西條芳文

Proceeding of 8th Sendai Symposium on Ultrasonic Tissue Characterization

November 11, 2005
Institute of Development, Aging and Cancer
Tohoku University

Symposium Chairman:
Yoshifumi Saijo, MD, PhD (Tohoku University)

Greeting from the Chairman

It is our great pleasure to host 8th Sendai Symposium on Ultrasonic Tissue Characterization again, this year. The symposium started in 1994 when Professor Motonao Tanaka retired from Tohoku University and held a sattelite symposium of World Federation for Ultrasound in Medicine and Biology which was held in Sapporo at that time.

The symposium was focused on ultrasonic tissue characterization. We invited Professors F. Dunn (University of Illinois), J. M. Thijssen (University of Nijmegen), J. G. Miller (Washington University), C. R. Hill (Royal Cancer Institute), J. Ophir (University of Texas), R C. Waag (University of Rochester), J. P. Jones (University of California, Irvine), S. Ohtsuki (Tokyo Institute of Technology), H. Hachiya (Tokyo Institute of Technology) H. Inoue (Akita University) to the symposium. Professors M. Tanaka, N. Chubachi, H. Kanai and Y. Saijo from Tohoku University also presented the papers.

It was originally scheduled as one day meeting but as traditional for Sendai conference, we had very hot discussions and extended the symposium to two-days meeting. After the symposium we published a monogram "Ultrasonic Tissue Characterization". However, it took another two years to publish it.

This year, we invited Professor Floyd Dunn from University of Illinois and Unversity of Arizona, and Professor A. F. W. van der Steen from Erasmus Medical Center Rotterdam to make heated discussion again. Each presentation is scheduled 15-minutes presentation and 15-minutes (and more) discussion. We decided to publish symposium proceeding for the second time for convinience for attendees and many researchers in this field all over the world.

We hope the symposium will produce some fruitful discussions and future international collaborations.

Sincerely,

Yoshifumi Saijo, MD, PhD

Department of Medical Engineering and Cardiology

Institute of Development, Aging and Cancer

Tohoku University

Program

10:00 Opening Remarks

Professor Floyd Dunn (University of Illinois, University of Arizona, Tohoku University)

10:05 Novel Approaches in Intravascular Ultrasound

Chair: Hiroshi kanai (Graduate School of Engineering, Tohoku University)

1. Parametric Intravascular Ultrasound Imaging

   Two-dimensional Tissue Velocity Imaging and Self-organizing Map Imaging

   Y. Saijo, E. Santos Filho, T. Yambe (Department of Medical Engineering and Cardiology Institute of Development, Aging and Cancer, Tohoku University)
   A. Tanaka (Faculty of Symbiotic Systems Science, Fukushima University)
   T. Iwamoto, M. Yoshizawa (Graduate School of Engineering, Tohoku University)
   Y. Akino, Y. Hanadate (Department of Cardiology, Miyagi Social Insurance Hospital)

2. Automatic Luminal Contour and Calcification Detection in Intravascular Ultrasound Images

   Esmeraldo dos Santos Filho (Graduate School of Engineering, Tohoku University)
   Yoshifumi Saijo (Institute of Development, Aging and Cancer, Tohoku University)
   Makoto Yoshizawa (Information Synergy Center, Tohoku University)
   Akira Tanaka (College of Symbiotic Systems Science, Fukushima University)

11:05 Precise Ultrasonic Measurement of Biological Materials

Chair: A. F. W. van der Steen (Erasmus Medical Center, Rotterdam)

3. Elasticity Imaging of Artery Wall for Transcutaneous Tissue Characterization

   Hideyuki Hasegawa, Jun Inagaki, Hiroshi Kanai (Department of Electronic Engineering, Graduate School of Engineering, Tohoku University)
   Masataka Ichiki (Sendai Hospital of East Railway Company)
   Fumiaki Tezuka (Sendai Medical Center)

4. Ultrasonic Measurement of Displacement Inside Object Caused by Dual Acoustic Radiation Force

   Mikito Takahashi, Hideyuki Hasegawa, and Hiroshi Kanai (Graduate School of Engineering, Tohoku University)

12:05 Lunch

13:00 Elasticity Measurement of Myocardium

Chair: Hideyuki Hasegawa (Graduate School of Engineering, Tohoku University)

5. Noninvasive Measurement of Myocardial Viscoelasticity

Hiroshi Kanai (Graduate School of Engineering, Tohoku University)

6. Measurement of Myocardial Strain Rate at High Temporal Resolution

Hiroki Yoshiara, Hideyuki Hasegawa, Hiroshi Kanai (Graduate School of Engineering, Tohoku University)

14:00 Development of Novel Acoustic Microscopy

Chair: Noriyoshi Chubachi (Tohoku Gakuin University)

7. Speed-of Sound Microscopy for Biomedical Applications

Y. Saijo, H. Sasaki, E. Santos Filho, T. Yambe, M. Tanaka (Institute of Development, Aging and Cancer, Tohoku University)
N.Hozumi (Toyohashi University of Technology)
K.Kobayashi (Honda Electronics Co.,Ltd)

8. Image processing for pulse driven biological microscope based on frequency spectrum

A. Kimura, S. Terauchi, Y. Murakami, N. Hozumi, M. Nagao, S. Yoshida (Toyohashi University of Technology)
K. Kobayashi (Honda Electronics Co.,Ltd)
Y. Saijo (Tohoku University)

15:30 Recent Applications of Acoustic Microscopy in Orthopedic Surgery

Chair: Naohiro Hozumi (Toyohashi University of Technology)

9. Increased Sound Speed of Synovial Membrane after Immobilization Assessed by Scanning Acoustic Microscopy

Yoshihiro Hagiwara, Fujio Matsumoto, Eiichi Chimoto, Shoichi Kokubun (Department of Orthopaedic Surgery, Tohoku University)
Yoshifumi Saijo (Institute of Development, Aging and Cancer, Tohoku University)
Yasuyuki Sasano(Division of Craniofacial Development and Regeneration, Tohoku University Graduate School of Dentistry)

10. Material Properties of the Rabbit Supraspinatus Tendon and its Insertion - A Measurement with the Scanning Acoustic Microscopy

Hirotaka Sano, Koshi Hattori, Shoichi Kokubun (Department of Orthopedic Surgery, Tohoku University)
Yoshifumi Saijo (Institute of Development, Aging and Cancer, Tohoku University)

17:00 Invited Lecture

Chair: Yoshifumi Saijo (Institute of Development, Aging and Cancer, Tohoku University)

Intravascular Ultrasound for Studying Atherosclerotic Plaque

Professor A. F. W. van der Steen (Department of Biomedical Engineering, Thorax Centre, Erasmus Medical Center, Rotterdam)

17:55 Closing Remarks

Professor Tomoyuki Yambe (Institute of Development, Aging and Cancer, Tohoku University)

Parametric Intravascular Ultrasound Imaging

Two-dimensional Tissue Velocity Imaging and Self-organizing Map Imaging

Y. Saijo, E. Santos Filho, T. Yambe
Department of Medical Engineering and Cardiology
Institute of Development, Aging and Cancer, Tohoku University
4-1 Seiryomachi, Aoba-ku, Sendai 980-8575, Japan
saijo@idac.tohoku.ac.jp

A. Tanaka
Faculty of Symbiotic Systems Science
Fukushima University
1 Kanayagawa, Fukushima 960-1296, Japan

T. Iwamoto, M. Yoshizawa
Graduate School of Engineering
Tohoku University
6-6-05 Aramaki-aza-Aoba, Aoba-ku, Sendai 980-8579, Japan

Y. Akino, Y. Hanadate
Department of Cardiology
Miyagi Social Insurance Hospital
143 Nakadamachi-aza-Maeoki, Taihaku-ku, Sendai 981-1103, Japan

Abstract— **We have been developing some methods for quantitative analysis of intravascular ultrasound (IVUS) imaging. In this paper, we present two-dimensional (2D) intravascular tissue velocity imaging and self-organizing map imaging. RF signal of 40-MHz IVUS apparatus was obtained by an A/D converter with sampling rate of 500-MSa-s. IVUS images were reconstructed from RF data sets and the images were divided into square shaped regions of interest (ROIs). The correlation and displacement of the ROIs between the consecutive two frames were calculated by template-matching method. Two-dimensional tissue velocity was defined as the vectors of displacement of ROI with 0.7 and more correlation. For self-organizing map (SOM) imaging, the frequency spectrum was calculated for each position of the hamming window using a mathematical autoregressive (AR) model. The optimized AR spectra were used to compute 18 spectral shape parameters for each ROI to construct SOM. Spectra were automatically classified into seven categories which may corresponded with catheter, guidewire shadow, blood, fibrosis, calcification, lipid, media and others.**

Keywords; intravascular ultrasound, tissue velocity imaging, self organizing map, coronary artery, atherosclerosis

I. INTRODUCTION

Intravascular ultrasound (IVUS) has been clinically applied since early 1990's and it has become an important clinical tool for investigation of coronary artery during percutaneous transluminal coronary intervention (PCI) therapies. IVUS is mainly used to measure the luminal and vascular areas and to confirm the full expansion of the coronary stent to the arterial wall. Besides the measurement of dimensions, IVUS also provides important information on tissue character of atherosclerosis.

First objective of the present study is to develop an algorithm for two-dimensional tissue velocity vector and strain of coronary artery. Second objective is to develop self-organizing map (SOM) imaging based on spectral analysis of radiofrequency (RF) signal for automatic plaque classification.

II. METHODS

A. RF Data Acqisuition

A commercial available IVUS system (Clear View Ultra, Boston Scientific, USA) was equipped. The central frequency of the IVUS probe (Atlantis SR Pro, Boston Scientific, USA) was 40 MHz and the pulse repetition rate was 7680 Hz. A single frame of the IVUS system consisted of 256 lines so that 7680 pulses made 30 f/s. An analogue to digital (A/D)

converter board (CompuScope 8500, Gage, USA) was connected to the RF output of the IVUS apparatus. The sampling rate was 500 MSa/s, the resolution was 8-bit and the on-board memory was 8 MB. Intra-coronary pressure was measured by fluid-filled method using 6 French (approximately 2.0 mm) diameter guiding catheter which was inserted into coronary artery. Biological signals such as electrocardiogram and intra-coronary pressure were simultaneously recorded using an A/D converter (PCI-6024E, National Instruments, USA) with the sampling rate of 100 kSa/s and the resolution of 12-bit [1].

After the RF data were sent to the workstation, the signals were pre-treated for further analyses. As the original RF signal consisted of one line, the data was divided into 10 matrixes. Each matrix consisted of 3053 lines by 256 columns and processed for one frame of IVUS image.

B. 2D Tissue Velocity Imaging

First, 30 to 50 MHz component of the original RF signal was extracted by using a software-based bandpass filtering method. Second, the original signal consisting of one line was divided into 10 matrixes. Each matrix consisted of 3053 lines by 256 columns and processed for one frame of IVUS image.

Ideally, one frame consisting of 256 lines of the rotational IVUS is equivalent to that of phased-array IVUS. However, a conventional rotating IVUS system uses frame trigger to adjust frame to frame rotational dis-uniformity. This indicates the position of the 'n/256'th line is not guaranteed to be at the same position of the previous frame. Then the correlation coefficient between two consecutive matrixes was calculated in the rotational direction and the rotational dis-uniformity was corrected in rotational direction to obtain the maximum correlation coefficient.

Conventional IVUS image was generated by converting polar coordinate of original RF signal matrix to rectangular coordinate. Then the IVUS image was divided into 64 by 64 square shaped regions of interest (ROIs). Pattern matching method was applied for calculation of correlation and displacement of the ROIs between the consecutive two frames.

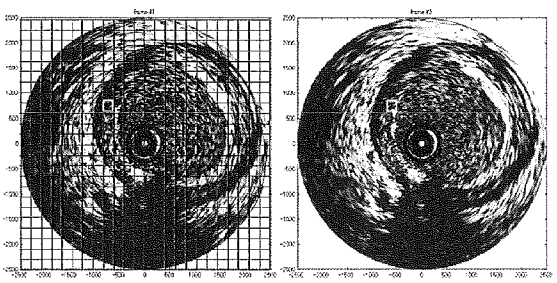

Figure 1. Re-construced IVUS images and segmentation

Figure 1 shows the reconstructed IVUS image (left) divided into 64 by 64 square shaped regions of interest. If the position of the center of the ROI (white highlighted square in the left image) is p (x_0, y_0) and the center of matched ROI (white highlighted square in the right image) is in the next frame is q (x_1, y_1), the displacement vector v is defined as

$$\vec{v} = (x_1 - x_0, y_1 - y_0) \cdots (1)$$

Two-dimensional tissue velocity was defined as the vectors of displacement divided by 33 ms (interval of two consecutive frames). The correlation between the two frames was high when the tissues were remained nearly same positions during 33 ms. We assumed that the ROI with 0.7 and more correlation coefficient was vascular wall. Tissue velocity vectors with the correlation more than 0.7 were overlaid on the conventional IVUS image. Figure 2 shows the correlation (left) and 2D tissue velocity imaging.

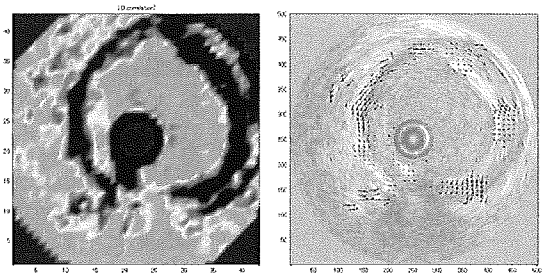

Figure 2. Correlation (left) and 2D tissue velocity imaging (right)

Tissue strain was defined as the change of the ROI area between two frames.

C. Self-organizing Map

1) Pre-treatment of the data

IVUS data were acquired with a commercially available IVUS system with the central frequency of 40MHz. RF data were digitized and stored in a workstation using by an A/D board with the sampling frequency of 500Msa/s and the resolution of 8 bits. Initially, a software-based band-pass filter (15MHz-105MHz) was applied to the IVUS RF signal data. Then each line in the ROI was scanned by a 128-points width hamming window. The frequency spectrum was calculated for each position of the hamming window using fast Fourier transform (FFT) and a mathematical autoregressive (AR) model. Akaike's final prediction error method estimated the optimum AR model order was 15 for characterizing plaque components. Figure 3 shows the raw RF signal wavelet consisted of 128 points. Figure 4 is the FFT and Figure 5 is the AR model.

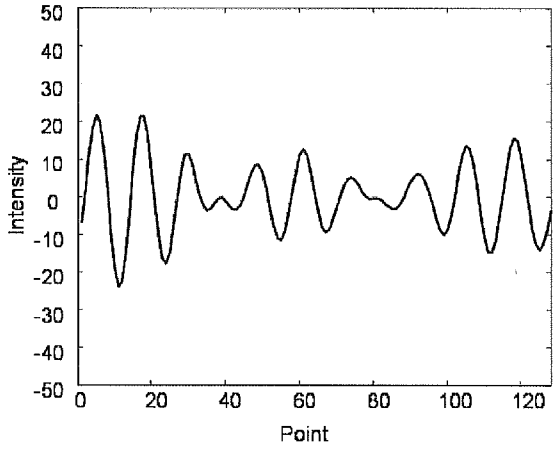

Figure 3. Raw RF data with 128 points

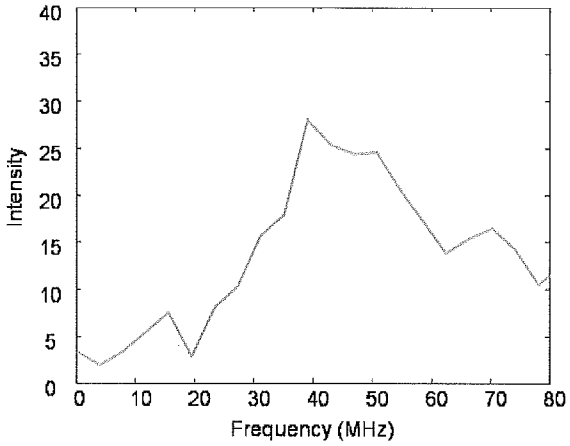

Figure 4. Spectrum calculated by FFT

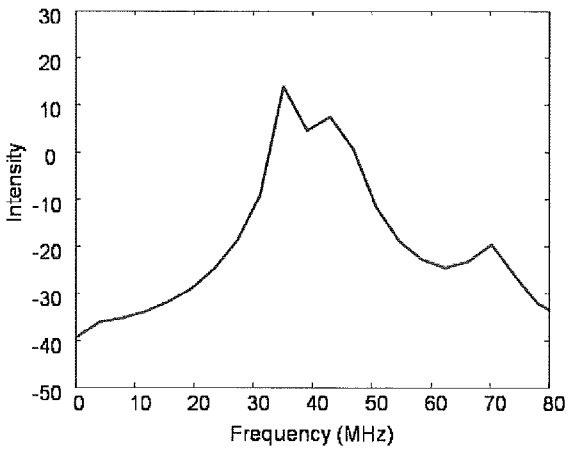

Figure 5. Spectrum calculated by AR method

Further, the optimized AR spectra were used to compute 18 spectral shape parameters for each ROI. These parameters were: 1. power and 2. frequency of fundamental wave, 3. power and 4. frequency of second harmonic wave, 5. local minimum power between fundamental wave power and second harmonic wave power, 6. frequency of local minimum power, 7. maximum power, 8. frequency of maximum power, 9. slope from power at frequency 15MHz to fundamental wave power, 10. corresponding y-intercept, 11. slope from fundamental wave power to local minimum power, 12. corresponding y-intercept, 13. slope from local minimum power to second harmonics power, 14. corresponding y-intercept, 15. slope from second harmonics power to 100MHz power, 16. corresponding y-intercept, 17. mean of integrated backscatter, and 18. ROI position at line.

2) SOM

The SOM is one of neural network application and it is a vector quantization method that places the weight vectors on a regular low-dimensional grid in an ordered fashion. A SOM consists of neurons organized on a regular grid. Each neuron is a d-dimensional weight vector where d is equal to the dimension of the input data vectors. The neurons are connected to adjacent neurons by a neighborhood relation, which dictates the topology, or structure, of the map.

In this study, the SOM classifier learned the spectral parameters for training. And then the SOM classifier classified windowed area of IVUS data based on these parameters. Finally, the tissue maps were reconstructed on IVUS B-mode images based on the SOM.

III. RESULTS

Figure 6 shows an example of color-coded IVUS image, correlation, 2D tissue velocity, 2D tissue strain and corresponded coronary tissue obtained by directional coronary atherectomy (DCA).

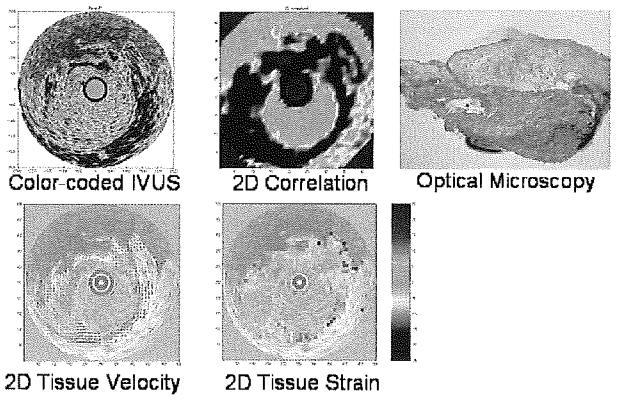

Figure 6. Color-coded IVUS image, correlation, 2D tissue velocity, 2D tissue strain and corresponded coronary tissue obtained by DCA

2D tissue velocity and strain are heterogeneous in this lesion and the optical microscopy shows the collagen-rich

fibrosis, smooth muscle, necrotic core and thrombus. The inhomogeneity of the sample is well represented by 2D tissue velocity and strain imaging.

Figure 7 is the SOM of the training data sets. Eighteen spectral parameters consisted 18-dimensional data were represented on a 2-dimensional map. In this way, the SOM classified the RF spectrum into seven categories. Figure 8 is the conventional IVUS image (left) and color-coded image based on automatic classification by SOM (right).

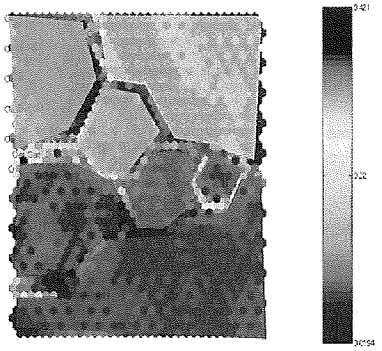

Figure 7. SOM classified the RF spectra into seven categories. 18-dimensional parameters were displayed on a 2-dimensional map.

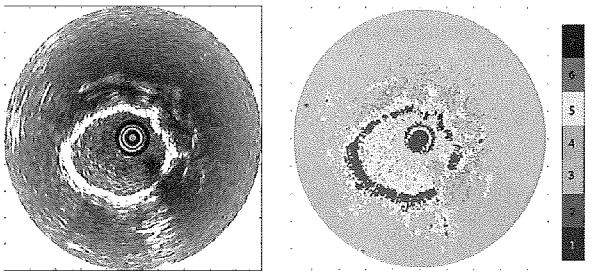

Figure 8. Conventional IVUS image (left) and color-coded image based on automatic classification by SOM (right)

IV. Discussion

The group at Erasmus University lead by van der Steen and de Korte has been applying correlation analysis technique to obtain vascular elasticity information using phased array IVUS system [2-4] because RF-line pairs between two consecutive frames are always guaranteed as coming from the same position of the tissue. Correlation analysis using rotating IVUS has been considered as difficult but the present study showed that correlation image clearly identified the vascular wall of coronary artery. The two-dimensional tissue velocity and strain derived by the method provide important information on tissue character. A vulnerable plaque showed heterogeneous strain indicating the tissue components are also inhomogeneous.

Virtual histology® (VH) has been clinically applied technique to classify coronary plaque into four categories. The technique is also based on RF spectral analysis. By our SOM analysis, the spectra were classified into seven categories which may corresponded with catheter, guidewire shadow, blood, fibrosis, calcification, lipid, media and others. Integration of these two techniques and introduction of the micro acoustic properties measured by acoustic microscopy may develop the algorithm.

V. Conclusions

We have developed two novel image analysis algorithms for IVUS. 2D tissue strain imaging corresponded well to the DCA-excised histological specimen. SOM analysis automatically classified the RF spectra of the IVUS image and it may provide additional information of the tissue character besides conventional gray-scale imaging to cardiologists.

Acknowledgments

This study was supported by Grants-in-Aid for Scientific Research (Scientific Research (B) 15300178, Scientific Research (B) 15360217) from the Japan Society for the Promotion of Science and Health and Labor Sciences Research Grants from the Ministry of Health, Labor and Welfare for the Research on Advanced Medical Technology (H17-Nano-001).

References

[1] Y. Saijo, A. Tanaka, N. Owada, Y. Akino, S. Nitta. Tissue velocity imaging of coronary artery by rotating-type intravascular ultrasound. Ultrasonics. 42(2004), pp. 753-757.

[2] A.F. van der Steen, C.L. de Korte, E.I. Cespedes. Intravascular ultrasound elastography. Ultraschall Med. 19(1998), pp.196-201.

[3] C.L. de Korte, G. Pasterkamp, A.F. van der Steen, H.A. Woutman, N. Bom. Characterization of plaque components with intravascular ultrasound elastography in human femoral and coronary arteries in vitro. Circulation 102 (2000), pp. 617-623.

[4] C.L. de Korte, M.J. Sierevogel, F. Mastik, C. Strijder, J.A. Schaar, E. Velema, G. Pasterkamp, P.W. Serruys, A.F. van der Steen. Identification of atherosclerotic plaque components with intravascular ultrasound elastography in vivo: a Yucatan pig study. Circulation 105 (2002), pp.1627-30.